Absorption and Emission of the Apigenin and Luteolin Flavonoids: A TDDFT Investigation†

Anna Amat,‡ Catia Clementi,‡ Filippo De Angelis,§ Antonio Sgamellotti,‡,§ and Simona Fantacci*,§

Dipartimento di Chimica, Università degli Studi di Perugia, via Elce di Sotto 8, I-06123 Perugia, Italy and Istituto di Scienze e Tecnologie Molecolari del CNR (CNR-ISTM), c/o Dipartimento di Chimica, via Elce di Sotto 8, I-06123 Perugia, Italy

Received: June 4, 2009; Revised Manuscript Received: August 6, 2009

The absorption and emission properties of the two components of the yellow color extracted from weld (*Reseda luteola* L.), apigenin and luteolin, have been extensively investigated by means of DFT and TDDFT calculations. Our calculations reproduce the absorption spectra of both flavonoids in good agreement with the experimental data and allow us to assign the transitions giving rise to the main spectral features. For apigenin, we have also computed the electronic spectrum of the monodeprotonated species, providing a rationale for the red-shift of the experimental spectrum with increasing pH. The fluorescence emission of both apigenin and luteolin has then been investigated. Excited-state TDDFT geometry optimizations have highlighted an excited-state intramolecular proton transfer (ESIPT) from the 5-hydroxyl to the 4-carbonyl oxygen of the substituted benzopyrone moiety. By computing the potential energy curves at the ground and excited states as a function of an approximate proton transfer coordinate for apigenin, we have been able to trace an ESIPT pathway and thus explain the double emission observed experimentally.

Introduction

Weld, extracted from *Reseda luteola* L., is the oldest natural dye known in Europe, and its use is traced back to the beginning of the Christian Era.[1−4] Many ancient books such as *Plichto* and *Le Teinturier parfait* report *Reseda luteola* L. as the best dyeing plant to fix yellow on silk and wool.[3,4] Besides textile dyeing, weld was also widely used as a pigment (lake) in painting and in medieval manuscripts.[5] In both applications, metal cations were used as a mordant to fix and stabilize the color on the fiber or inorganic substrate (generally chalk or hydrated alumina) through complexation and precipitation processes. Weld optical properties are due to the flavonoids contained in the plant, more specifically luteolin and apigenin (ratio 9:1). (See Scheme 1.) Flavonoids are characterized by a 2-phenyl-1,4-benzopyrone skeleton and are usually classified in terms of the number and position of the hydroxyl substituents, following this classification apigenin and luteolin are named 5,7,4′-trihydroxyflavone and 5,7,3′,4′-tetrahydroxyflavone, respectively.

In the last few decades, a growing interest on flavonoids has been demonstrated because of a large spectrum of biological and pharmaceutical properties[6−11] such as their well-known antioxidant activity.[6−8] Interestingly, in very recent applications, these natural dyes have been used as an alternative to synthetic photosensitizers in dye-sensitized solar cells.[12,13]

Despite the large number of experimental studies on the antioxidant properties of apigenin and luteolin, only a recent paper by Favaro et al.[2] has reported an exhaustive spectrophotometric and fluorometric study of the two main components of the yellow color extracted from weld. The maxima of the lowest-energy absorption band of apigenin and luteolin measured in MeOH−water (1/2, *v*/*v*) at acidic pH were found at 337 and at 348 nm, respectively. Apigenin exhibits a weak excitation-dependent double emission in methanol ($\phi_f = 4 \times 10^{-4}$) with a maximum at 430 nm and a shoulder at 534 nm when the system is excited at 300 nm, whereas only a maximum at 534 nm is retrieved when the system is excited at 357 nm. This double emission seems to be related to excited-state intramolecular proton transfer (ESIPT) from the phenolic O_5 to the carbonilic O_4.[2] Natural occurring flavones, possessing several OH groups, often show ESIPT. For example, 3-hydroxylflavone, showing a five-membered hydrogen bond, has been taken as a prototype for studying the dynamics of the proton transfer on the excited state,[14−16] even though many of these natural flavonoids have a glycoside moiety linked to the C_3 position, which hampers ESIPT.[17] Controversial results have been found for the ESIPT in 5-hydroxyflavone (5HF), which has, however, been deeply studied both experimentally and theoretically.[17−21] For luteolin, no emission is detectable because the fluorescence quantum yield is lower than 10^{-4}.[2] The absorption spectrum of weld extract in methanol is very similar to that of luteolin, which is, in fact, the main dye component, whereas the fluorescence behavior is determined by apigenin.

For polyphenol systems, optical properties might be strongly dependent on the nature of the solvent and on the solution pH. In the paper by Favaro et al., the acido- and iono-chromic properties of apigenin and luteolin have been studied as a crucial step to individuate the processes responsible for the color changes with aging, which is of particular interest in the diagnostics and conservation of works of art. The absorption spectra of apigenin and luteolin progressively shifts toward longer wavelengths as the pH solution increases up to 437 and 402 nm, respectively. Moreover, deprotonation leads to an enhancement of the emission intensity of both flavonoids, and thus luteolin fluorescence becoming detectable.

Despite the numerous experimental works on flavones, only a few theoretical studies have been reported to date that deal with the structural and acid−base properties of luteolin[22−25] and

† Part of the "Vincenzo Aquilanti Festschrift".

* Corresponding author. E-mail: simona@thch.unipg.it.
‡ Università degli Studi di Perugia.
§ Istituto di Scienze e Tecnologie Molecolari del CNR (ISTM-CNR).

10.1021/jp9052538
Published on Web 09/01/2009

SCHEME 1: Luteolin and Apigenin Structures and Atom Labels

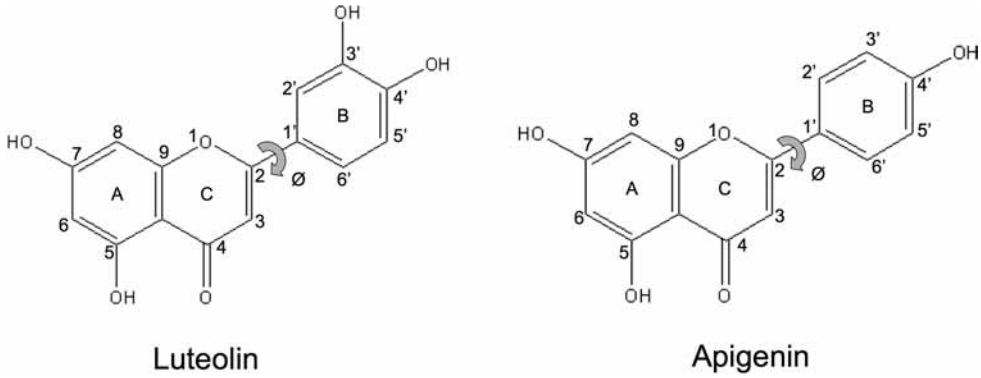

apigenin.[23,24] In this article, a theoretical investigation on the optical properties of apigenin and luteolin by means of density functional theory (DFT) and time-dependent DFT (TDDFT) methods is reported. After a calibration of the computational procedure, in terms of choice of basis set, exchange-correlation functional, and solvation model, the absorption spectra of the two dyes have been simulated, thus assigning the nature of the excited states involved in the absorption process. Moreover, because understanding color alterations with the pH changes can be crucial for conservation purposes, we have also investigated the acid−base properties of apigenin and the changes in its absorption spectrum passing from the neutral form to the deprotonated form. Finally, we have focused our attention on the apigenin fluorescence. In its lowest excited state, marked changes in the geometry related to the ESIPT have been computed, which is in agreement with the large measured Stokes shift. We hypothesized an excited-state decay mechanism through the molecule planarization and an internal proton transfer that provides a rationale for the double emission experimentally detected.

Computational Methodology. Calculations of the apigenin and luteolin absorption spectra have been carried out by means of TDDFT,[26−28] as implemented in the G03 package.[29] Preliminary TDDFT calculations have been performed on apigenin to set up the methodology to be used; the computed spectra using different xc functionals and basis sets are compared with the absorption experimental spectrum, and all results are reported in the Supporting Information. In particular, pure DFT functionals have been tested with the Perdew, Burke, and Ernzerhof exchange-correlation functional, PBE[30,31] and have been compared with hybrid functionals such as the PBE0[32] and the widely used B3LYP (Becke's hybrid exchange functional B3[33] with the Lee−Yang−Parr correlation functional LYP[34,35]).

Geometry optimizations with no symmetry constraints have been carried out using the different xc functionals combined with different basis sets, and TDDFT calculations have been performed on the computed geometries at the same level of theory. The lowest 40 singlet−singlet excitations have been computed and transition energies and oscillator strengths have been interpoled using a Gaussian convolution with a σ of 0.20.

Effects of the solvation, water, and methanol have been taken into account by means of the conductor-like polarizable continuum model (CPCM)[36−39] using the UAHF solvation radii.[40]

These calibration calculations on apigenin have shown the crucial role of the solvent in describing the spectroscopic properties of this class of compounds and that the tested B3LYP and PBE0 hybrid functionals satisfactorily reproduce the experimental absorption spectra, whereas the PBE functional provides a red-shifted spectrum. This is probably due to the underestimation of the SCF HOMO−LUMO gap, which is not fully corrected in the TDDFT excitation energies.[41] Neither the inclusion of further diffuse functions nor the increase in the basis set result in significant improvements on the calculations (Supporting Information), which is consistent with the results recently reported by Jacquemin et al.[42] on the simulation of dyes optical properties. Therefore, B3LYP and the 6-31+g*[43−45] basis set, that give a good performance at a reasonable computational cost, have been used in all of calculations.

To investigate the emission process, we have computed the geometries of the first excited state of both flavonoids by TDDFT using B3LYP and the TZVP[46,47] basis set with the Turbomole package.[48] We have obtained the potential-energy curves related to the proton transfer from O_5 to O_4 on the ground and the lowest excited states by freezing the O_5H coordinate from 0.850 to 1.950 Å in steps of 0.050 Å and optimizing the rest of the coordinates in vacuo. The solvation effects have been subsequently included on the ground- and excited-state curves using B3LYP/6-31+g*//CPCM. Notably, no relevant differences have been found between the apigenin ground-state geometries computed with Turbomole and G03 both in vacuo and in solution. (See the Supporting Information.) We have obtained a projection of the absorption/emission energies along the O_5H coordinate by computing the lowest singlet−singlet excitation on the ground-state-/lowest-exited-state-optimized geometries using B3LYP/6-31+g*//CPCM.

Results and Discussion

Electronic Structure and Absorption Spectrum of Apigenin. The experimental absorption spectrum was measured in a MeOH−water mixture (1/2, *v*/*v*) in a highly acidic environment (pH 2) to ensure the absence of anionic species. To rationalize solvent effects in the apigenin absorption process, we have performed calculations in vacuo, methanol, and water solutions. Molecular structures are not strongly affected by the presence of the solvent, and optimized geometrical parameters are very similar both in vacuo and in water and methanol solvents.[24] No significant differences in terms of geometry, molecular orbitals (MOs) energy and character, or computed spectrum (Supporting Information) have been retrieved between water and methanol calculations; therefore, only results obtained in water will be reported. Whereas the frontier molecular orbitals of apigenin in vacuo and in water solution do not show relevant differences in energy and only slight changes in character, remarkable differences are observed between the absorption spectra computed in vacuo and in solution. (See Figure 1a,b and the Supporting Information.) (Hereafter we will refer to

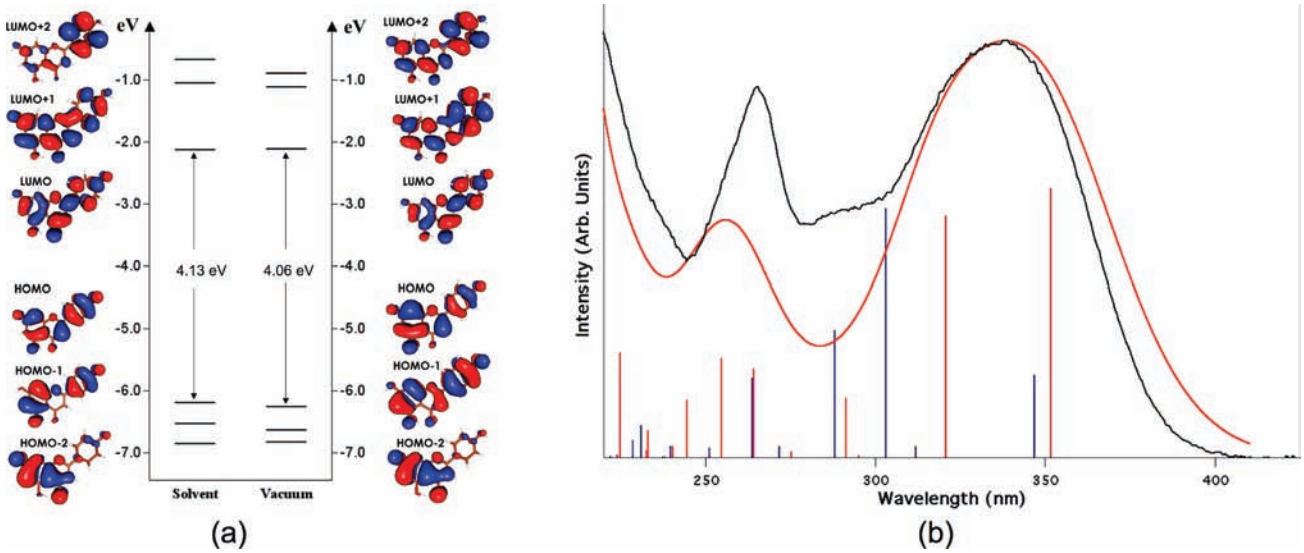

Figure 1. (a) Apigenin frontier molecular orbital energies and isodensity plots in water and in vacuo. (b) Apigenin experimental spectrum (black) compared with computed spectra in water (red), together with computed singlet−singlet transitions in water (red) and in vacuo (blue).

the highest occupied molecular orbital, HOMO, and the lowest unoccuppied molecular orbital, LUMO, as H and L, respectively).

As previously found,[24] the HOMOs of apigenin in solution have an overall π-bonding character. The H and H-2 show a partial nonbonding character because of the carbonilic oxygen lone pair. Whereas in the H, the charge is completely delocalized in the H-1 is mainly localized in rings A and B, and the H-2 is mainly localized in the 1,4-benzopyrone moiety with a minimum involvement of the B ring. The H computed in vacuo shows a larger charge localization on the ring A with respect to that computed in water; the H-1 in vacuo introduces a π-bonding component on the C ring. The LUMOs in water have an overall antibonding π^* character with the charge delocalized all over the molecule. In particular, the L is highly delocalized and has an overall π^* character, except for the bonding contribution between the $C_8-C_9-C_{10}-C_5$ and the $C_{1'}-C_2$ connecting the 1,4-benzopyrone with the phenyl ring B. The L+1 has an antibonding π^* character, which does not show the bonding contribution within the A ring as the L and presents only some bonding contribution between the B ring and the rest of the molecule involving the $O_1-C_2-C_{1'}-C_{2'}$ atoms. The L and L+1 in water and vacuo are very similar.

A part these slight character differences, the described MOs, are quite similar in vacuo and in solution, and the H−L gap is only 0.08 eV higher in vacuo; nevertheless, the absorption spectra computed in vacuo and in solution present relevant differences. In Figure 1b, the comparison between the experimental[2] and the computed absorption spectra of apigenin in water together with the related transitions in water and in vacuo is reported. The experimental main absorption band measured at 337 nm is computed at 338 nm in water, whereas the main absorption band is computed in vacuo at 299 nm, with a pronounced shoulder at 347 nm. (See the Supporting Information.) Therefore, the agreement between the experimental and computed in water spectra is very good, while the spectrum in vacuo is not consistent with the experimental data, pointing out, as we already observed for transition-metal complexes, the importance of solvent effects to reproduce accurately the experimental spectra.[49,50] Interestingly, whereas for the transition-metal complexes, we attributed the discrepancy between vacuo and solvent to the electronic structure differing both in terms of energy and nature of the frontier orbitals, for apigenin, given the similar energy and character of the frontier molecular orbitals, the differences between vacuo and solvent have to be ascribed to the response part of the calculations.

Further insight into the origin of the different absorption spectra computed in vacuo and solution may be obtained by analyzing the computed transitions that give rise to the main absorption bands of the spectrum in terms of energy, oscillator strength, and involved molecular orbitals, both in vacuo and in solution, and comparing them with the main experimental absorption maxima. (See Table 1.) To visualize the charge transfer associated with the lowest-energy transitions, both in vacuo and in solution, we report in Figure 2 the isodensity plots of the electron density difference between S_1, S_2, S_3, and the ground state (S_0); blue (white) color refers to a decrease (increase) in the electron density upon excitation. Transition dipole moments and dipole moments associated with the three lowest excitations have been computed and reported in the Supporting Information.

From an analysis of the TDDFT eigenvectors computed in water, the band experimentally measured at 337 nm is composed of two transitions, $S_0 \rightarrow S_1$ and $S_0 \rightarrow S_2$, of similar intensity calculated at 352 and 321 nm, resulting in a computed band centered at 338 nm. Both transitions have as arriving state the L and as starting states the H and H-1 with inverse percentage contributions. $S_0 \rightarrow S_1$ shows an electron density flow from the A to the B and C rings, whereas $S_0 \rightarrow S_2$ accounts for a charge transfer toward the C ring. (See Figure 2.) Considering the nature of the molecular orbitals involved in these transitions, the resulting band can be assigned to a $\pi \rightarrow \pi^*$ absorption. We are also able to relate the dim signal of the experimental spectrum at 302 nm to a weak transition computed at 291 nm. This transition has the L as the final state and the H-2 as the initial state. Because the H-2 is mainly localized in the AC ring moiety, this transition has a partial charge transfer character from the AC ring to the phenyl ring B, resulting in a totally delocalized excited state. (See Figure 2.) In the higher-energy region, two $\pi \rightarrow \pi^*$ transitions are computed, which, analogous to the two lowest-energy transitions, have as starting states H and H-1 but L+1 as the arriving state.

As mentioned above, not all experimental features are correctly reproduced by calculations in vacuo. To investigate

TABLE 1: Apigenin Experimental and Theoretical Absorption Maxima (nanometers), Computed Transitions (nanometers/electronvolt), Oscillator Strength (*f*), and Composition in Terms of Molecular Orbitals with the Related Character in Water (left) and Vacuo (right)

exptl max (nm)	theor max (nm)	theor (nm/eV)	*f*	MO	theor max (nm)	theor (nm/eV)	*f*	MO
337	338	352/3.52 (S_1)	0.41	(81%) H → L ($\pi \rightarrow \pi^*$) (9%) H-1 → L ($\pi \rightarrow \pi^*$)	347(sh)	347/3.58 (S_1)	0.13	(87%) H → L ($\pi \rightarrow \pi^*$) (5%) H-1 → L ($\pi \rightarrow \pi^*$)
		321/3.86 (S_2)	0.38	(83%) H-1 → L ($\pi \rightarrow \pi^*$) (7%) H → L ($\pi \rightarrow \pi^*$)		312/3.98 (S_2)	0.02	(86%) H-3 → L (n → π^*) (5%) H-2 → L (n → π^*)
		295/4.20 (S_3)	0.00	(86%) H-4 → L (n → π^*) (5%) H-2 → L (n → π^*)	299	303/4.09 (S_3)	0.38	(66%) H-1 → L ($\pi \rightarrow \pi^*$) (15%) H-2 → L (n → π^*)
302	291	291/4.25 (S_4)	0.09	(72%) H-2 → L (n → π^*) (12%) H → L+1 ($\pi \rightarrow \pi^*$)		288/4.30 (S_4)	0.20	(59%) H-2 → L (n → π^*) (13%) H-1 → L ($\pi \rightarrow \pi^*$) (11%) H → L+1 ($\pi \rightarrow \pi^*$)
		275/4.50 (S_5)	0.01	(62%) H-3 → L (n → π^*) (19%)H → L+2 ($\pi \rightarrow \pi^*$) (8%) H → L+1 ($\pi \rightarrow \pi^*$)		272/4.56 (S_5)	0.02	(47%) H → L+1 ($\pi \rightarrow \pi^*$) (23%) H-4 → L (n → π^*) (10%) H → L+2 ($\pi \rightarrow \pi^*$)
268	256	264/4.69 (S_6)	0.14	(54%) H → L+1 ($\pi \rightarrow \pi^*$) (11%) H-1 → L+1 ($\pi \rightarrow \pi^*$) (10%) H-2 → L (n → π^*)	264(sh)	264/4.70 (S_6)	0.12	(22%) H → L+1 ($\pi \rightarrow \pi^*$) (20%) H-1 → L+1 ($\pi \rightarrow \pi^*$) (17%) H-4 → L (n → π^*)
		255/4.87 (S_7)	0.15	(66%) H-1 → L+1 ($\pi \rightarrow \pi^*$) (14%) H → L+1 ($\pi \rightarrow \pi^*$)		251/4.94 (S_7)	0.01	(51%) H → L+2 ($\pi \rightarrow \pi^*$) (14%) H-1 → L+2 ($\pi \rightarrow \pi^*$) (13%) H-4 → L (n → π^*)

that further, we focus on the lowest electronic excitations, comparing $S_0 \rightarrow S_1$, $S_0 \rightarrow S_2$, and $S_0 \rightarrow S_3$ computed in vacuo with those in water. Whereas the $S_0 \rightarrow S_1$ transition in vacuo is comparable to the corresponding excitation in water, the $S_0 \rightarrow S_2$ transition in vacuo, which involves H-3 and L orbitals, has a negligible oscillator strength and can be related to $S_0 \rightarrow S_3$ in water, and vice versa $S_0 \rightarrow S_3$ in vacuo ($f = 0.38$), with the most relevant contribution coming from H-1 → L transition, corresponds to $S_0 \rightarrow S_2$ in water.

The $S_0 \rightarrow S_1$ transition is computed at similar energies (within 0.05 eV) and accompanied by similar charge density flow (Figure 2) in vacuo and in water. Its oscillator strength, however, is appreciably lower in vacuo than in water (0.13 vs 0.41). The $S_0 \rightarrow S_2$ (water) and $S_0 \rightarrow S_3$ (vacuum) transitions show H-1 → L as the main contribution with 83 and 66%, respectively, with a 15% of H-2 → L contribution calculated in vacuo. This can be easily visualized by the isodensity plots of the electron density difference associated with these transitions, which essentially differ for the distribution of the starting states involving different parts of A ring. (See Figure 2.) The $S_0 \rightarrow S_2$ (water) and $S_0 \rightarrow S_3$ (vacuum) transitions differ in energy by 0.23 eV, showing, however, the same oscillator strength. For the sake of completeness we also computed the charge flows associated with $S_0 \rightarrow S_3$ (water)/$S_0 \rightarrow S_2$ (vacuum), confirming an almost identical spatial distribution and negligible oscillator strength.

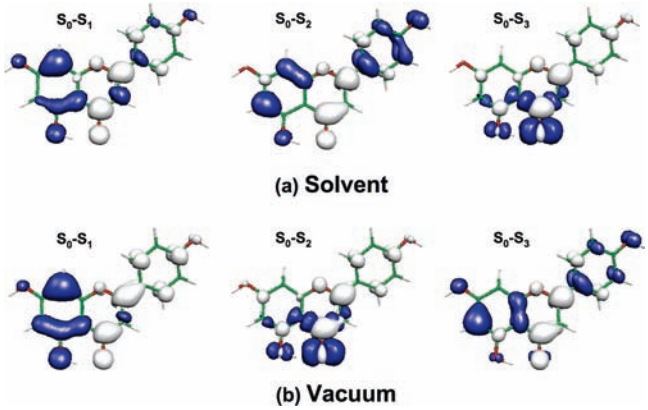

Figure 2. Isodensity plots of the electron density difference between S_0-S_1, S_0-S_2, and S_0-S_3 of apigenin computed (a) in water solution and (b) in vacuo. A blue (white) color indicates a decrease (increase) in the electron density upon excitation.

In summary, in vacuo, the $S_0 \rightarrow S_1$ and $S_0 \rightarrow S_3$ excitations are computed more energetically spaced with respect to the corresponding transitions in solution and with an oscillator strength ratio of 0.13:0.38 with respect to 0.41:0.38 for the water case; these differences translate into a spectrum with the main absorption band at 299 nm and a pronounced shoulder at 347 nm, which is in disagreement with the experiment and calculations in solution. The agreement between the experimental spectrum and that computed in water and in methanol (Supporting Information) is very good. We are able to reproduce all of the main experimental features and to assign the first experimental absorption band as a superposition of two singlet−singlet transitions.

Luteolin Absorption Spectrum and Electronic Structure. Using the same methodology applied to apigenin, the luteolin absorption spectrum has been simulated and compared with the experimental result.[2] The electronic structure of luteolin is very similar to that of apigenin (Figure 3a), as previously reported.[24] TDDFT results are shown in Figure 3b and Table 2, and they are again in good agreement with the experiment; the lowest computed absorption band is only slightly rigidly red-shifted with respect to the experimental one.

The similarities observed between luteolin and apigenin both in the transition energies and their composition are not surprising because of the resemblance of the two systems and their electronic structures. (See Figures 1a and 3a.) The main difference experimentally detected, the red-shift of the luteolin absorption spectrum with respect to apigenin, is also retrieved in our calculations, even though it is slightly overestimated (0.20 versus 0.11 eV), and can be rationalized by the destabilization of the luteolin H-1 and the H,[24] reflected also into the H-L gap decrease, 3.90 eV with respect to the 4.13 eV of apigenin. The two lowest transitions, essentially H → L and H-1 → L excitations, are computed at 361 and 331 nm, 0.08 and 0.12 eV lower than those computed for apigenin. Analogous to apigenin, the main experimental band at 348 nm is formed by these two transitions of $\pi \rightarrow \pi^*$ character, but the luteolin S_2 transition computed at 331 nm is less intense than the one at 361 nm, 0.10 versus 0.54, whereas for apigenin, the intensity ratio is 0.38:0.41, which implies that in luteolin the computed band is practically centered on the lowest transition. Regarding the character of the orbitals (Figures 1a and 3a) involved in the two lowest transitions, the only remarkable difference explaining the different oscillator strength of apigenin/luteolin transitions

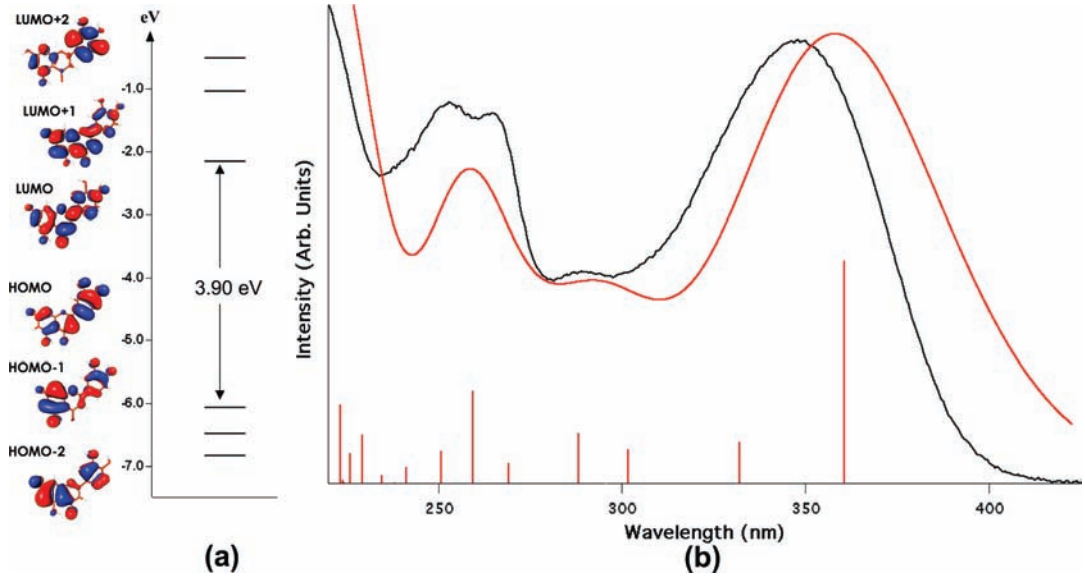

Figure 3. (a) Luteolin frontier molecular orbital energies and isodensity plots in water. (b) Luteolin experimental spectrum (black) compared with computed spectrum in water (red).

TABLE 2: Luteolin Experimental and Theoretical Absorption Maxima (nanometers), Computed Transition with an Oscillator Strength Higher than 0.05 (nanometers/electronvolt), Oscillator Strength and Composition in Terms of Molecular Orbitals with the Related Character

exptl (nm)	theor max (nm)	theor (nm/eV)	f	MO
348	358	361/3.44 (S_1)	0.54	(81%) H → L ($\pi \rightarrow \pi^*$)
				(7%) H-1 → L ($\pi \rightarrow \pi^*$)
		331/3.74 (S_2)	0.10	(86%) H-1 → L ($\pi \rightarrow \pi^*$)
				(6%) H → L ($\pi \rightarrow \pi^*$)
290	292(sh)	302/4.11 (S_3)	0.08	(76%) H-2 → L (n → π^*)
				(12%) H-3 → L ($\pi \rightarrow \pi^*$)
		288/4.30 (S_5)	0.12	(68%) H-3 → L ($\pi \rightarrow \pi^*$)
				(8%) H-2 → L (n → π^*)
				(6%) H-1 → L ($\pi \rightarrow \pi^*$)
266−253	258	269/4.61 (S_6)	0.05	(81%) H → L+1 ($\pi \rightarrow \pi^*$)
		259/4.78 (S_7)	0.22	(73%) H-1 → L+1 ($\pi \rightarrow \pi^*$)
		251/495 (S_8)	0.08	(55%) H → L+2 ($\pi \rightarrow \pi^*$)
				(14%) H-5 → L ($\pi \rightarrow \pi^*$)
				(9%) H-2 → L+1(n → π^*)

is the presence in the luteolin H-1 of an electronic distribution involving $C_{6'}-C_{1'}-C_2-C_3$ atoms from the B to C rings. For luteolin, the experimental feature detected at 290 nm is computed at 292 nm (Table 2 and Figure 3b), and it is formed by two transitions computed at 302 and 288 nm, having as arriving state L and as starting states H-2 and H-3, respectively. In the high-energy region, three transitions are computed at 269, 259, and 251 nm, which give rise to the experimental band measured at 253 nm and a shoulder at 266 nm.

Monodeprotonated Apigenin Absorption Spectrum. Because of the acido-chromic behavior of weld, the absorption spectra of apigenin and luteolin were experimentally studied as a function of pH in the 2−12 pH range.[2] For luteolin, three acid−base dissociation steps were individuated, characterized by pK_a values of 6.9, 8.6, and 10.3, whereas for apigenin, pK_a values of 6.6 and 9.3 were detected. The absorption spectra of both flavonoids are markedly red-shifted by increasing the pH, which translates into an enhancement of the yellow color.

To gain insight into the electronic structure changes occurring upon the first deprotonation, we have investigated the absorption spectrum of the monodeprotonated apigenin. Also, in this case, the results obtained for apigenin can be extended to luteolin. We previously established a suitable integrated DFT-MP2 (MP2*) methodology to compute the pK_a for luteolin and other polyphenolic compounds[25] on the basis of the combination of the MP2 energies and geometries in vacuo and in solution with thermal contributions calculated by DFT. For luteolin, we found the presence of three OH groups, which are in strong competition for deprotonation. On the contrary, apigenin presents a more well-defined deprotonation site because of the impossibility of forming intramolecular hydrogen bonds upon deprotonation in the B ring. Therefore, we calculated the pK_a values of all the possible apigenin deprotonation sites at the MP2* level. We find pK_a values of 7.44, 8.66, and 11.60 for positions 7, 4′, and 5, respectively. (See the Supporting Information for complete results.) These results allow us to undertake the study of the spectral modifications with increasing pH by relating the experimental absorption spectrum of the monodeprotonated species to the deprotonated apigenin in position 7. Using the same methodology as that applied in the neutral case, the red-shift experimentally observed upon deprotonation is qualitatively retrieved, although it appears to be strongly overestimated. (See Figure 4.) In fact, the main transition, entirely responsible in our calculations for the first absorption band, is computed at 414 nm and is red-shifted by 0.33 eV with respect to the experimental maximum measured at 372 nm. We have also tested a larger basis set and different hybrid functionals without obtaining any improvement in the absorption spectrum (See the Supporting Information.) Charged species present, however, challenging difficulties in the treatment of the solute−solvent interactions because of the strong electrostatic effects that arise from unbalanced localized charges.[51] Sometimes the introduction of solvent effects with a polarizable continuum model is not sufficient for accurately describing the solute charge distribution, and the addition of explicit water molecules becomes necessary to take into account specific solute−solvent interactions. In the present case, the inclusion of one, three, and five explicit water molecules in the simulations gradually improves the results, mainly by stabilizing the H and increasing the H−L gap. We will report here only the results obtained for clusters with zero and five water molecules; for complete results with zero, one, three, and five water molecules, see the Supporting Information. Figure 4a presents the frontier orbital scheme along with H and L isodensity plots of anionic apigenin.

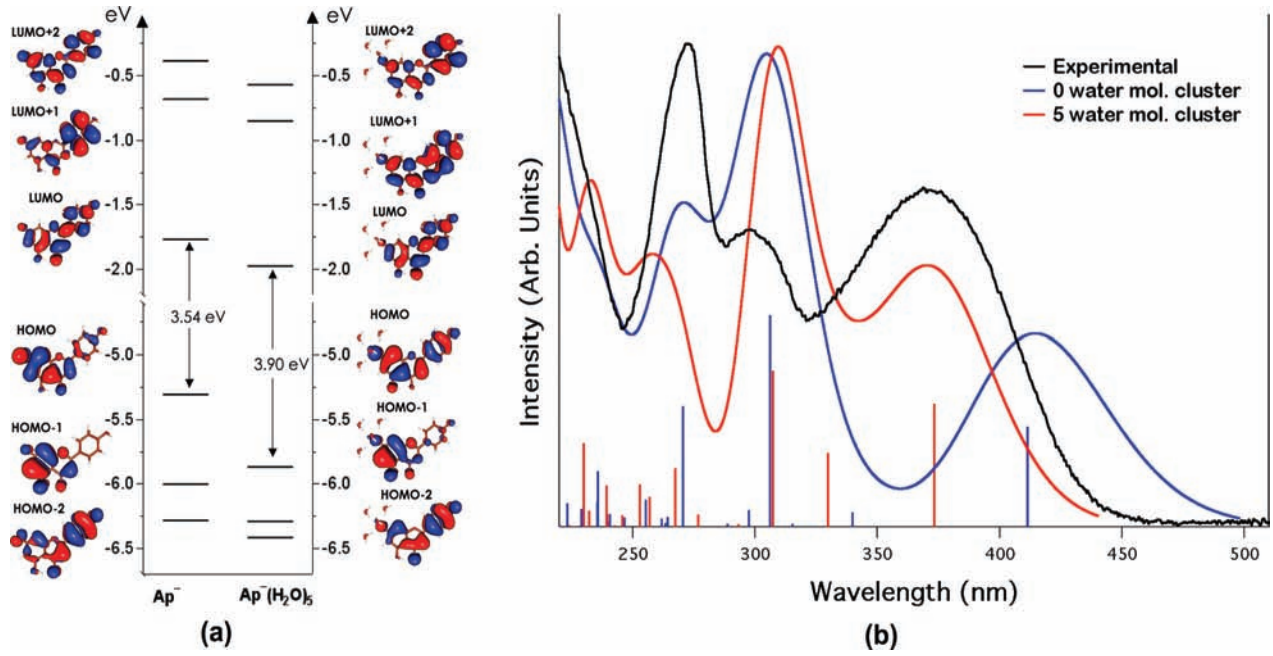

Figure 4. (a) Molecular orbital levels and isodensity plots of monodeprotonated apigenin with 0 (blue) and 5 (red) explicit water molecules. (b) Apigenin experimental spectrum at pH 8 (black) compared with computed spectra of the monodeprotonated apigenin cluster with 0 (blue) and 5 (red) explicit water molecules.

TABLE 3: Experimental (pH 8) and Theoretical Absorption Maxima (nanometers), Computed Transitions with an Oscillator Strength Higher than 0.05 (nanometers/electronvolt), Oscillator Strength, and Composition in Terms of Molecular Orbitals with the Related Character for the Mono-Deprotonated Apigenin with Five Explicit Water Molecules

exptl (nm)	theor max (nm)	theor (nm/eV)	*f*	MO
372	373	373/3.32 (S_1)	0.32	(89%) H → L ($\pi \rightarrow \pi^*$)
300	309	330/3.76 (S_2)	0.19	(87%) H-1 → L (n → π^*)
		307/4.03 (S_3)	0.41	(81%) H-2 → L ($\pi \rightarrow \pi^*$)
				(7%) H → L+1 ($\pi \rightarrow \pi^*$)
273	261	267/4.64 (S_6)	0.15	(25%) H → L+1 ($\pi \rightarrow \pi^*$)
				(23%) H-4 → L ($\pi \rightarrow \pi^*$)
				(19%) H-1 → L+1 (n → π^*)
				(6%) H → L+2 ($\pi \rightarrow \pi^*$)
		257/4.82 (S_8)	0.08	(47%) H-1 → L+1 (n → π^*)
				(13%) H → L+1 ($\pi \rightarrow \pi^*$)
				(9%) H → L+4 ($\pi \rightarrow \pi^*$)
		253/4.90 (S_9)	0.11	(66%) H → L+2 ($\pi \rightarrow \pi^*$)
				(13%) H-4 → L ($\pi \rightarrow \pi^*$)

The H−L gap is computed to increase steadily from 3.54 to 3.90 eV going from zero to five water molecules. Along with these variations in the H−L gap, an increase in the electron density in the B ring is retrieved for the H upon the addition of the water molecules, resulting in a completely delocalized orbital, whereas the L is almost unchanged.

The computed spectra of deprotonated apigenin using zero and five water molecules are compared with the experimental absorption spectrum in Figure 4b. For the $Ap^-(H_2O)_5$ system, the agreement with the experiment is good, even though the relative intensity of the transition computed at 307 nm is quite overestimated. We notice, however, that the relative intensities in the experimental data could also be affected by the presence of neutral species for which the 268 nm band is much more intense than the signal at 302 nm. The results for $Ap^-(H_2O)_5$ are summarized in Table 3; here we will only briefly discuss the assignment of the lowest-energy absorption bands.

The transition computed at 373 nm, which essentially gives rise to the experimental absorption band at 372 nm, is an H → L excitation with a $\pi \rightarrow \pi^*$ character and is the feature that is most affected by the deprotonation and consequently by the presence of water molecules. This is expected because the H is the predominant starting state of this electronic excitation. The transition computed at 330 nm of H-1 → L nature has a charge transfer character from the A/C rings to the B ring that reminds the one observed in the H-2 → L transition of the neutral apigenin. $S_0 \rightarrow S_1$ and $S_0 \rightarrow S_2$ transitions are more spaced in energy with respect to those corresponding to apigenin. On one hand, this could explain the different shape of the lowest absorption band of the spectrum measured at pH 8 with respect to that at pH 2; on the other hand, this could be partially responsible of the intensity overestimation of the computed spectral feature at 300 nm. The $S_0 \rightarrow S_3$ transition computed at 307 nm of H-2 → L nature fits fairly well with the corresponding experimental band measured at 300 nm. This excitation resembles in character the $S_0 \rightarrow S_2$ transition of the neutral species and also shows similar oscillator strengths. Finally, the experimental band measured at 273 nm is computed at 267 nm with a composition of several transitions of similar weight, and it seems to not be affected by pH increase. Overall, the computed spectrum of the monodeprotonated apigenin reproduces the main experimental spectral changes upon increasing the solution pH, in particular, the red-shift and the change in shape of the lowest absorption band.

Apigenin and Luteolin Emission. For apigenin, a weak double emission ($\Phi_F = 4 \times 10^{-4}$) with maxima at 430 and 534 nm has been measured in methanol solution.[2] The emission spectrum has been found to depend on the excitation wavelength: by exciting at 300 nm, the emission spectrum showed a maximum at 430 nm and a pronounced shoulder at 534 nm, whereas by exciting at 357 nm, only the latter red-shifted emission was recorded.[2] The low fluorescence quantum yield and the short lifetime of 0.8 ns suggest that the main deactivation pathways for the excited singlet state of apigenin are nonradiative.

To understand the emission process, we have optimized the geometry of both apigenin and luteolin lowest singlet excited state, S_1, by TDDFT. In Table 4, we report the main optimized

TABLE 4: Apigenin and Luteolin Main Geometrical Parameters of the Ground (S_0) and First Excited (S_1) States Computed Using B3LYP/TZVP

		O_4H	C_4O_4H	O_5H	C_5O_5H	$C_2C_{1'}$	θ
apigenin	S_0	1.692	100.2	0.997	106.7	1.468	18.2
	S_1	0.990	107.5	1.752	99.6	1.413	2.8
luteolin	S_0	1.690	100.2	0.997	106.6	1.468	17.6
	S_1	0.989	107.5	1.754	99.7	1.412	1.1

bond distances and angles for the S_1 and S_0 geometries. It is worth noting that for both apigenin and luteolin in the S_1 geometry an ESIPT occurs from the phenolic O_5 in the A ring to the ketonic O_4 in the C ring.

Apart from the different location of the proton, the main difference between the ground and excited state structures is related to the torsion angle $O_1C_2C_{1'}C_{2'}$ between the B and C rings. In the ground state, apigenin (luteolin) adopts a nonplanar structure with a dihedral angle of 18.2° (17.6°), whereas in the first singlet excited state, the molecule is almost planar, characterized by a dihedral angle of only 2.8° (1.1°).

To understand the ESIPT process in depth, for apigenin, we performed constrained geometry optimizations on both the S_0 and S_1 surfaces, selecting the O_5H distance as an approximate reaction coordinate. By varying the O_5H distance in the range of 0.8 to 1.9 Å, we explored the approximate ESIPT pathway. Calculation of the ground- and excited-state energies on the S_0 and S_1 geometries, allows us to draw a schematic representation of the ESIPT pathway. The results are collected in Figure 5.

The molecule is promoted by the absorption at 3.56 eV to the Franck−Condon (FC) point. Relaxation from FC at fixed O_5H distance leads to a planarization of the system along with a slight lengthening of the C−OH bonds with a 0.29 eV energy gain. Upon increasing of the O_5H distance, the energy decreases, reaching a minimum region for O_5H distances around 1.7 Å. Associated with this proton motion, a ca. 0.5 eV energy gain is computed. From the excited-state minimum, we calculate an emission energy of 1.88 eV, to be compared with an experimental emission maximum of 2.32 eV. The barrierless S_1 energy curve computed along the O_5H coordinate is suggestive of an ultrafast proton transfer in line with the one measured experimentally for 5HF.[17,18]

We also searched for a minimum structure on the S_1 curve in the flat energy region close to the FC point, but all of our attempts to locate such a minimum structure failed independently on the exchange-correlation functional used, leading to the O_4-bound tautomer. CIS calculations based on a Hartree−Fock ground state performed in solution evidenced a local minimum for the O_5-bound tautomer 0.12 eV above the more stable O_4-bound tautomer. Therefore, whereas the presence of the O_4-bound species is largely independent from the level of theory employed, the presence of a O_5-bound minimum is not confirmed by TDDFT. This result could be affected by an overestimated stabilization of the proton transfer for the excited state.[52−54]

The analysis of the ground-state energies shows an almost parallel behavior along the S_0 and S_1 curves, the latter lying as expected at higher energy. Both the S_0 and S_1 curves show a flat region in correspondence of the excited-state minimum, characterized by the presence of a very shallow minimum on the ground state for the apigenin form with the proton bound to O_4. This O_4-tautomer structure observed in the S_0 curve has been optimized and characterized by the calculation of all positive frequencies as a local minimum computed 0.27 eV above the global O_5-bound minimum.

The above results allow us to interpret the experimental picture. After excitation to the FC point, the system undergoes a planarization, followed by or concomitant to the ESIPT from the O_5 to the O_4 bound tautomer. From the O_4 tautomer the system emits, providing the 534 nm emission found experimentally. The flat energy region around the FC point and the possible presence of an O_5-bound excited state minimum, as calculated by CIS, would be consistent with the emission experimentally found at 430 nm being originated by an excited state with a geometry close to the ground-state minimum structure with the proton bound to O_5. Finally, the presence of a shallow minimum on the ground state in correspondence with the O_4-bound tautomer might explain the sensitivity of the apigenin emission to the excitation wavelength. Indeed, by exciting at low energy, this O_4-bound tautomer would lead to exclusively low-energy emission from the corresponding excited-state O_4-bound species because the system cannot surmount the ca. 0.50 eV that is necessary to reach the O_5-bound tautomer.

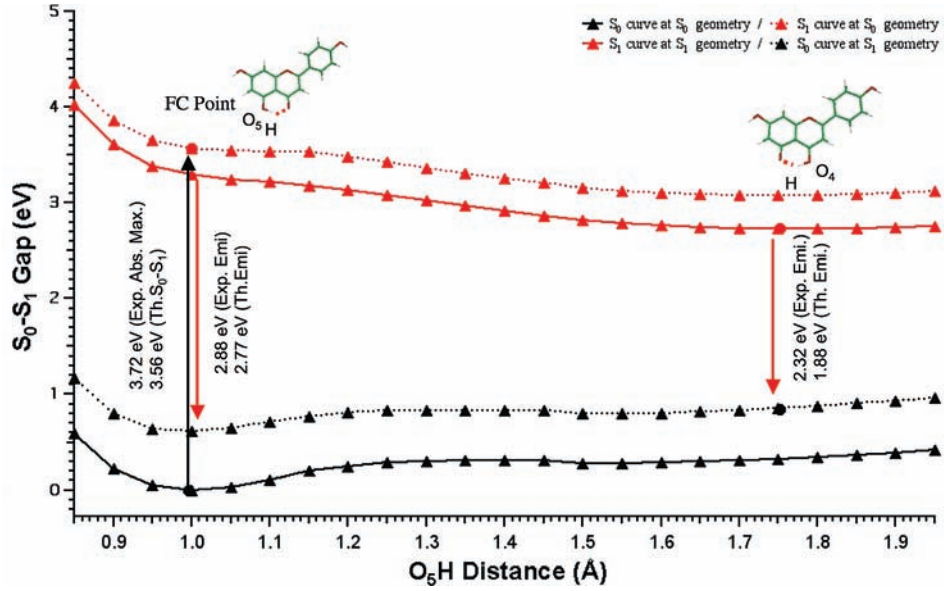

Figure 5. Apigenin proton transfer potential energy curve at different O_5H fixed distances for the ground (S_0) and first excited (S_1) states.

On the basis of these results, we can describe the absorption process as an FC transition from the apigenin ground state to its S_1 excited state. A first relaxation process is undertaken through the planarization of the molecule, thus allowing a first emission computed at 2.77 eV with a computed Stokes shift of 0.90 eV, which is in good agreement with the measured fluorescence at 430 nm (2.88 eV) and Stokes shift of 0.84 eV. In a second process driven by the C_5O_5 and C_4O_4 bending modes between 250 and 270 cm^{-1}, the almost barrierless proton transfer takes place with a 0.54 eV energy gain, reaching the O_5-bound tautomer minimum of the excited state curve. From this point, a second emission occurs, giving rise to the fluorescence computed at 1.88 eV. This second emission is underestimated with respect to the experimental value of 2.32 eV, probably because of an overestimated stabilization of the proton transfer on the excited state, as previously observed.[52−54] We also remark that this value could be improved by taking into account the vibronic effects by calculation of the FC factors.[55,56]

The luteolin emission spectrum has not experimentally been measured because of a very low quantum yield. For luteolin, we performed a partial S_1 geometry optimization by fixing the O_5H distance at the S_0 optimized value. Similarly to apigenin, after an absorption process described in our approach as a vertical transition, a first relaxation occurs that is mainly ruled by the planarization of the molecule; from this point, the molecule can (i) deactivate to S_0 by nonradiative processes, (ii) deactivate to S_0 by emission at 2.73 eV, and (iii) start the proton transfer process driven by the C_5O_5 and C_4O_4 bending modes reaching the S_1 minimum, where a second emission can take place at 1.85 eV.

Conclusions

We have reported a theoretical study on the absorption and emission properties of apigenin and luteolin, the two main components of the yellow color extracted from *Reseda luteola* L.. These flavonoids were investigated by means of DFT and TDDFT calculations to rationalize several aspects of their experimentally observed optical properties. After calibrating the computational methodology, we simulated the absorption spectra of apigenin and luteolin, finding a very good agreement with the experiment, both in terms of maxima energy and overall spectral shape. The necessity of including solvation effects to describe the absorption spectra accurately has been discussed, demonstrating that the main differences between vacuo and solution results are ascribed to the response part of the calculations because the electronic structures computed in vacuo and in water/methanol are very similar. TDDFT eigenvectors analysis has allowed us to assign the experimental absorption spectra; we found that the low-energy absorption band at 337 (348) nm for apigenin (luteolin) is composed of two rather separate transitions of $\pi-\pi^*$ character computed at 352 and 321 (361 and 331) nm, the latter showing a partial charge transfer character.

The effect of increasing the solution pH on the apigenin absorption spectrum has been evaluated by simulating the absorption spectrum of the monodeprotonated species. This task has followed the theoretical assignment of apigenin pK_a values, which has allowed us to individuate the first deprotonation as occurring at the 7-hydroxyl site. The experimental red-shift of the apigenin spectrum upon increasing the pH is mainly related to a red-shift of the lowest excitation forming the first absorption band. This sensitivity to pH is mainly related to a HOMO destabilization; this orbital has sizable localization on the A ring, where deprotonation occurs.

To investigate the emission process, we have performed TDDFT optimization of the lowest excited state for both apigenin and luteolin and have found an excited-state-optimized structure characterized by an intramolecular proton transfer, ESIPT. To trace an approximate proton transfer pathway, we have computed the potential-energy curves on S_0 and S_1 as a function of the O_5H distance. Our results suggest that upon excitation apigenin is promoted to the FC point from which a first relaxation process occurs through a planarization of the molecule. From the FC region, the excited-state energy decreases rapidly up to a flat region corresponding to the ESIPT minimum structure. In correspondence with this excited-state minimum, we have computed for apigenin an emission energy of 1.88 eV to be compared with the experimental value of 2.32 eV. Although no local minimum structure has been calculated by TDDFT in the flat energy region around the FC point, the presence of an O_5-bound excited-state minimum calculated by CIS suggests that the fluorescence experimentally measured at 2.88 eV, calculated at 2.77 eV, might be due to emission from an excited-state structure that has not yet undergone the ESIPT process.

Overall, our results suggest that careful DFT/TDDFT calculations in solution represent a valuable tool to interpret the acid−base and excited-state properties of flavones, thus opening the way for further comprehension of the physical−chemical properties of this important class of molecules, with particular reference to the color changes taking place with aging and under different environment conditions.

Acknowledgment. We thank Dr. Costanza Miliani, Dr. Aldo Romani, and Prof. Brunetto Giovanni Brunetti for helpful discussions. Work supported by the project Eu-ARTECH (CT-2004-506171), ST@RT and "Laboratorio di Diagnostica di Spoleto, Italy".

Supporting Information Available: Apigenin computed spectra at different levels of calculation; apigenin S_0 main geometrical parameters at different levels of calculation; apigenin frontier MO energies computed in water and methanol solution; apigenin computed transitions, oscillator strengths, and composition in methanol solution; apigenin dipole moments for S_0, S_1, and S_2 computed in water and in vacuo; apigenin transition dipole moments for $S_0 \rightarrow S_1$, $S_0 \rightarrow S_2$, and $S_0 \rightarrow S_3$ excitations computed in water and in vacuo; computed contributions to ΔG_s for the pK_a calculations of monodeprotonated apigenin in position 7, 4′, and 5; monodeproptonated apigenin spectra computed at different levels of calculation; monodeprotonated apigenin frontier molecular orbital energies and isodensity plots for clusters with zero, one, three, and five explicit water molecules; and monodeprotonated apigenin computed absorption spectra for clusters with zero, one, three, and five water molecules. This material is available free of charge via the Internet at http://pubs.acs.org.

References and Notes

(1) Forbes, R. J. *Studies in Ancient Technology*; E. J. Brill: Leiden, The Netherlands, 1964; Vol. IV.
(2) Favaro, G.; Clementi, C.; Romani, A.; Vickackaite, V. *J. Fluoresc.* **2007**, *17*, 707–714.
(3) Leix, A. *Färberei im Mittelalter*, Ciba Rundschau 1, 1936.
(4) Hofenk de Graaf, J. H. *The Colourful Past*; Archetype Publications, Ltd.: London, U.K., 2004.
(5) Saunders, D.; Kirby, J. *Natl. Gallery Tech. Bull.* **1994**, *15*, 79–97.
(6) van Acker, S. A. B. E.; de Groot, M. J.; van den Berg, D. J.; Tromp, M. N. J. L.; Donne-OpdenKelder, G.; van der Vijgh, W. J. F.; Bast, A. *Chem. Res. Toxicol.* **1996**, *9*, 1305–1312.
(7) Burda, S.; Oleszek, W. *J. Agric. Food Chem.* **2001**, *49*, 2774–2779.

(8) Leopoldini, M.; Russo, N.; Chiodo, S.; Toscano, M. *J. Agric. Food Chem.* **2006**, *54*, 6343–6351.
(9) Van Acker, S. A. B. E.; Van Den Berg, D. J.; Tromp, M. N. J. L.; Griffioen, D. H.; Van Bennekom, W. P.; Van Der Vijgh, W. J. F.; Bast, A. *Free Radical Biol. Med.* **1996**, *20*, 331–342.
(10) Panda, S.; Kar, A. *J. Pharm. Pharmacol.* **2007**, *59*, 1543–1548.
(11) Galicka, A.; Nazaruk, J. *Int. J. Mol. Med.* **2007**, *20*, 889–895.
(12) Calogero, G.; Di Marco, G. *Sol. Energy Mater. Sol. Cells* **2008**, *92*, 1341–1346.
(13) Meng, S.; Ren, J.; Kaxiras, E. *Nano Lett.* **2008**, *8*, 3266–3272.
(14) Dick, B.; Ernsting, N. P. *J. Phys. Chem.* **1987**, *91*, 4261–4265.
(15) Strandjord, A. J. G.; Courtney, S. H.; Friedrich, D. M.; Barbara, P. F. *J. Phys. Chem.* **1983**, *87*, 1125–1133.
(16) Gormin, D.; Sytnik, A.; Kasha, M. *J. Phys. Chem. A* **1997**, *101*, 672–677.
(17) Chou, P. T.; Chen, Y. C.; Yu, W. S.; Cheng, Y. M. *Chem. Phys. Lett.* **2001**, *340*, 89–97.
(18) del Valle, J. C. *J. Chem. Phys.* **2006**, *124*, 104506–104519.
(19) Norikane, Y.; Itoh, H.; Arai, T. *J. Photochem. Photobiol., A* **2004**, *161*, 163–168.
(20) Falkovskaia, E.; Sengupta, P. K.; Kasha, M. *Chem. Phys. Lett.* **1998**, *297*, 109–114.
(21) Martinez, M. L.; Studer, S. L.; Chou, P. T. *J. Am. Chem. Soc.* **1991**, *113*, 5881–5883.
(22) van Acker, S.; de Groot, M.; van den Berg, D. J.; Tromp, M.; Donne-OpdenKelder, G.; van der Vijgh, W.; Bast, A. *Chem. Res. Toxicol.* **1996**, *9*, 1305–1312.
(23) Leopoldini, M.; Pitarch, I.; Russo, N.; Toscano, M. *J. Phys. Chem. A* **2004**, *108*, 92–96.
(24) Amat, A.; De Angelis, F.; Sgamellotti, A.; Fantacci, S. *THEOCHEM* **2008**, *868*, 12–21.
(25) Amat, A.; De Angelis, F.; Sgamellotti, A.; Fantacci, S. *Chem. Phys. Lett.* **2008**, *462*, 313–317.
(26) Stratmann, R. E.; Scuseria, G. E.; Frisch, M. J. *J. Chem. Phys.* **1998**, *109*, 8218–8224.
(27) Bauernschmitt, R.; Ahlrichs, R. *Chem. Phys. Lett.* **1996**, *256*, 454–464.
(28) Casida, M. E.; Jamorski, C.; Casida, K. C.; Salahub, D. R. *J. Chem. Phys.* **1998**, *108*, 4439–4449.
(29) Frisch, M. J.; Trucks, G. W.; Schlegel, H. B.; Scuseria, G. E.; Robb, M. A.; Cheeseman, J. R.; Montgomery, J. A., Jr.; Vreven, T.; Kudin, K. N.; Burant, J. C.; Millam, J. M.; Iyengar, S. S.; Tomasi, J.; Barone, V.; Mennucci, B.; Cossi, M.; Scalmani, G.; Rega, N.; Petersson, G. A.; Nakatsuji, H.; Hada, M.; Ehara, M.; Toyota, K.; Fukuda, R.; Hasegawa, J.; Ishida, M.; Nakajima, T.; Honda, Y.; Kitao, O.; Nakai, H.; Klene, M.; Li, X.; Knox, J. E.; Hratchian, H. P.; Cross, J. B.; Adamo, C.; Jaramillo, J.; Gomperts, R.; Stratmann, R. E.; Yazyev, O.; Austin, A. J.; Cammi, R.; Pomelli, C.; Ochterski, J. W.; Ayala, P. Y.; Morokuma, K.; Voth, G. A.; Salvador, P.; Dannenberg, J. J.; Zakrzewski, V. G.; Dapprich, S.; Daniels, A. D.; Strain, M. C.; Farkas, O.; Malick, D. K.; Rabuck, A. D.; Raghavachari, K.; Foresman, J. B.; Ortiz, J. V.; Cui, Q.; Baboul, A. G.; Clifford S.; Cioslowski, J.; Stefanov, B. B.; Liu, G.; Liashenko, A.; Piskorz, P.; Komaromi, I.; Martin, R. L.; Fox, D. J.; Keith, T.; Al-Laham, M. A.; Peng, C. Y.; Nanayakkara, A.; Challacombe, M.; Gill, P. M. W.; Johnson, B.; Chen, W.; Wong, M. W.; Gonzalez, C.; Pople, J. A. *Gaussian03*, revision A.1; Gaussian, Inc.: Pittsburgh, PA, 2003.
(30) Perdew, J. P.; Burke, K.; Ernzerhof, M. *Phys. Rev. Lett.* **1996**, *77*, 3865–3868.
(31) Perdew, J. P.; Burke, K.; Ernzerhof, M. *Phys. Rev. Lett.* **1997**, *78*, 1396.
(32) Adamo, C.; Barone, V. *J. Chem. Phys.* **1999**, *110*, 6158–6170.
(33) Becke, A. D. *J. Chem. Phys.* **1993**, *98*, 5648–5652.
(34) Lee, C.; Yang, W.; Parr, R. G. *Phys. Rev. B.* **1998**, *37*, 785–789.
(35) Miehlich, B.; Savin, A.; Stoll, H.; Preuss, H. *Chem. Phys. Lett.* **1989**, *157*, 200–206.
(36) Barone, V.; Cossi, M. *J. Phys. Chem. A* **1998**, *102*, 1995–2001.
(37) Cossi, M.; Rega, N.; Scalmani, G.; Barone, V. *J. Comput. Chem.* **2003**, *24*, 669–681.
(38) Cossi, M.; Barone, V. *J. Phys. Chem. A* **2000**, *104*, 10614–10622.
(39) Cossi, M.; Barone, V. *J. Chem. Phys.* **2001**, *115*, 4708–4717.
(40) Barone, V.; Cossi, M.; Tomasi, J. *J. Chem. Phys.* **1997**, *107*, 3210–3221.
(41) Jacquemin, D.; Perpete, E. A.; Scuseria, G. E.; Ciofini, I.; Adamo, C. *J. Chem. Theory Comput.* **2008**, *4*, 123–135.
(42) Jacquemin, D.; Perpete, E. A.; Ciofini, I.; Adamo, C. *Acc. Chem. Res.* **2009**, *42*, 326–334.
(43) Rassolov, V. A.; Ratner, M. A.; Pople, J. A.; Redfern, P. C.; Curtiss, L. A. *J. Comput. Chem.* **2001**, *22*, 976–984.
(44) Rassolov, V. A.; Pople, J. A.; Ratner, M. A.; Windus, T. L. *J. Chem. Phys.* **1998**, *109*, 1223–1229.
(45) Clark, T.; Chandrasekhar, J.; Spitznagel, G. W.; Schleyer, P. v. R. *J. Comput. Chem.* **1983**, *4*, 294–301.
(46) Eichkorn, K.; Weigend, F.; Treutler, O.; Ahlrichs, R. *Theor. Chim. Acta* **1997**, *97*, 119–124.
(47) Schäfer, A.; Huber, C.; Ahlrichs, R. *J. Chem. Phys.* **1994**, *100*, 5829–5835.
(48) Ahlrichs, R.; Bär, M.; Häser, M.; Horn, H.; Kölmel, C. *Chem. Phys. Lett.* **1989**, *162*, 165–169.
(49) Fantacci, S.; De Angelis, F.; Selloni, A. *J. Am. Chem. Soc.* **2003**, *125*, 4381–4387.
(50) Fantacci, S.; De Angelis, F.; Sgamellotti, A.; Re, N. *Chem. Phys. Lett.* **2004**, *396*, 43–48.
(51) Kelly, C. P.; Cramer, C. J.; Truhlar, D. G. *J. Phys. Chem. A* **2006**, *110*, 2493–2499.
(52) Aquilanti, V.; Capecchi, G.; Cavalli, S.; Adamo, C.; Barone, V. *Phys. Chem. Chem. Phys.* **2000**, *2*, 4095–4103.
(53) Mijoule, C.; Latajka, Z.; Borgis, D. *Chem. Phys. Lett.* **1993**, *208*, 364–368.
(54) Aquino, A.; Lischka, H.; Hattig, C. *J. Phys. Chem. A* **2005**, *109*, 3201–3208.
(55) Dierksen, M.; Grimme, S. *J. Chem. Phys.* **2004**, *120*, 3544–3554.
(56) Improta, R.; Barone, V.; Santoro, F. *Angew. Chem.* **2007**, *46*, 405–408.

JP9052538